

**B. Enaux · V. Granet · O. Vermorel ·  
C. Lacour · L. Thobois · V. Dugué ·  
T. Poinsot**

# **Large Eddy Simulation of a motored single-cylinder piston engine: numerical strategies and validation**

Received: date / Revised: date

**Abstract** This paper describes a compressible Large Eddy Simulation (LES) used to investigate cyclic variations for nonreacting flow in an optical single cylinder engine setup. The simulated operating point is part of a large experimental database designed to validate LES for cycle-to-cycle prediction, and constitutes a first step towards the realization of fired operating points. The computational domain covers almost the whole experimental setup (intake and exhaust plenums, intake and exhaust ducts, cylinder) to account for acoustic phenomena. The assessment of the computation is performed in two regions of the domain: the intake and exhaust duct predictions are compared to the results of a Helmholtz solver and the experiment (pressure transducers and Particle Image Velocimetry (PIV)) while the in-cylinder dynamics are confronted to PIV measurements. The ability of the developed methodology to capture the correct level of cycle-to-cycle variations

---

B. Enaux  
CERFACS, CFD Team, 42 Avenue G. Coriolis, 31057 Toulouse Cedex 01, France  
PSA Peugeot Citroën - DRIA, 2 Route de Gisy, 78943 Velizy-Villacoublay Cedex, France

V. Granet  
CERFACS, CFD Team, 42 Avenue G. Coriolis, 31057 Toulouse Cedex 01, France  
Renault SAS, 1 Avenue du Golf, 78288 Guyancourt Cedex, France

O. Vermorel  
CERFACS, CFD Team, 42 Avenue G. Coriolis, 31057 Toulouse Cedex 01, France  
E-mail: Olivier.Vermorel@cerfacs.fr

C. Lacour  
IFP, 1 & 4 Avenue de Bois-Préau, 92852 Rueil-Malmaison Cedex, France

L. Thobois  
PSA Peugeot Citroën - DRIA, 2 Route de Gisy, 78943 Velizy-Villacoublay Cedex, France

V. Dugué  
Renault SAS, 1 Avenue du Golf, 78288 Guyancourt Cedex, France

T. Poinsot  
Université de Toulouse, IMFT, France

is demonstrated considering in-cylinder pressure and velocity fields predictions. Cycle-to-cycle variations in velocity are highlighted and localized using a proper orthogonal decomposition analysis.

**Keywords** Internal combustion engine · Multi-cycle Large-Eddy Simulation · Cycle-to-cycle variations · Unstructured grids · Acoustic

## 1 Introduction

A major challenge for the development of Internal Combustion (IC) engines is to improve fuel economy and to reduce pollutant emissions while maintaining or enhancing engine performances. New strategies using stratified charge direct injection or downsizing with high levels of exhaust gas recirculation have this potential, but can impact on the combustion stability and trigger high Cycle-to-Cycle Variations (CCV).

Nowadays Computational Fluid Dynamic (CFD) applied to engine development mainly relies on the Reynolds Averaged Navier Stokes (RANS) approach which solves ensemble or phase-averaged mean quantities. However, this method does not provide information about individual cycles. The study of cycle-to-cycle variability is thus impossible and other numerical methods such as LES (Large Eddy Simulation) must be employed. LES of laboratory-scale but also real turbulent combustors, such as gas turbine chambers, have recently appeared in the literature [29, 2, 34, 13]. In comparison to numerous publications related to gas turbines for example, LES of IC engines is still a field to explore.

Two major reviews, one by Haworth [20] and the other by Celik *et al.* [5], summarize the work accomplished by the LES engine community. They both highlight the potential of LES for predicting the details of the transient in-cylinder flow dynamics and demonstrate that LES is able to produce superior predictions than any of the current RANS approaches. They also support the view that LES can provide essential information in regard to the nature and origins of CCV. However, they both underline that computational cost is a major shortcoming that LES will have to overcome to ensure its practical use. Indeed, by nature, CCV can only be studied by performing multiple cycles and statistical analysis. 25 cycles are reported to be a minimum for a correct sampling in terms of mean values and 50 cycles are probably necessary to yield reliable statistics in terms of fluctuations [21, 4]. Fortunately, the constant increase in computational resources and the use of massively parallel machines now make such computations realistic.

Several multi-cycle LES-based computations have been reported in the literature since the review papers of Haworth [20] and Celik *et al.* [5]. Hasse *et al.* [19] performed 13 consecutive cycles of a motored engine using Detached Eddy Simulation (DES). Cycle-to-cycle velocity fluctuations at the spark plug were investigated at the time of ignition. It was shown that the differences in velocity could lead to significant combustion variations when computing the corresponding reacting case. Considering 5 different initial scenarios, Goryntsev *et al.* [14, 15] performed 10 consecutive nonreacting two-phase flow LES cycles for each scenario. It was found that CCV phenomena were directly linked to turbulence and that velocity cyclic variations had a great impact on the fuel-air mixing process. Multi-cycle simulations of fired operating points have also been performed recently [37,

---

43,46]. In particular, it was shown in [46] that LES was able to reproduce the experimental trend in terms of CCV, even with only 9 simulated cycles. In this study, the sources of CCV were investigated and the importance of the turbulence generated by the tumble breakdown was highlighted.

However, most authors highlight the lack of experimental data specifically dedicated to the validation of LES [5,9,46]. The French project SGEmac has been specially built to validate LES of CCV by acquiring a large experimental database on different operating points of a four-valve spark ignition engine [24]. This database includes motored engine and fired operating points, with low or high levels of CCV. A detailed characterization of the various operating points is achieved with numerous temperature and temporal pressure measurements at several locations of the set-up. Optical diagnostics (Particle Image Velocimetry (PIV), OH Laser Induced Fluorescence (LIF), combustion chemiluminescence) allow also the investigation of the local properties of the flow.

The computational domain includes most of the experimental setup: cylinder, intake and exhaust ducts, intake and exhaust plenums. This strategy has potentially two major drawbacks, its CPU cost since the computational domain is large ( $\sim 2.5$  m long) and its modeling cost since some additional devices (flame-arrestors for example) must be accounted for. But it also offers two great advantages: first, it allows to capture acoustic phenomena in the ducts which are a possible source of CCV [20,9,46]; second, it enables a proper definition of intake and exhaust boundary conditions. Indeed, in most studies, boundary conditions are imposed in the intake and exhaust ducts, close to the cylinder [14,37,46]. With such a compact domain, several challenging issues need to be tackled such as turbulence injection, back-flow treatment or acoustic wave reflection for instance. With an extended domain, these issues vanish naturally.

In this paper, only a motored engine case is reported. It constitutes an essential validation step before computing more complex operating points with combustion. This operating point is experimentally known to be very stable with low CCV. Therefore, the objective here is not only to discuss cyclic variations but also to prove that the chosen methodology is suitable to describe with high fidelity the engine behavior, from an aerodynamic and acoustic point of view. To ensure a proper statistical sampling of the flow field, 27 consecutive LES cycles are performed.

This paper is organized as follows. The experimental setup and engine settings are recalled in section 2. The LES solver and the models are presented in section 3. Section 4 describes the meshing methodology, the prescription of the boundary conditions and the modeling of the flame-arrestors. Section 5 presents a comparison of the LES results with PIV acquisitions and temporal pressure measurements specifically introduced in the experimental setup. The flow behavior in the intake and exhaust lines is first analyzed before considering the in-cylinder predictions.

## 2 Experimental setup

The SGEmac engine test bench operated at IFP has been specifically designed to investigate cyclic combustion variability. This single-cylinder is a four-valve, pent-roof, spark ignition engine with a flat piston. The whole setup is displayed in Fig. 1(a) and the main parameters are summarized in Table 1.

**Table 1** Characteristics of the SGEmac engine test bench. Crank Angle Degrees (*CAD*) are relative to compression Top-Dead-Center (TDC). The *CAD* of valve openings and closures correspond to experimental residual valve lifts of 0.1 mm.

|                             | Units          | Values |
|-----------------------------|----------------|--------|
| Compression ratio           | [-]            | 9.9    |
| Engine speed                | [rpm]          | 1200   |
| Bore                        | [mm]           | 82     |
| Stroke                      | [mm]           | 83.5   |
| Connecting rod length       | [mm]           | 144    |
| Intake Valve Opening (IVO)  | [ <i>CAD</i> ] | 350    |
| Intake Valve Closure (IVC)  | [ <i>CAD</i> ] | -120   |
| Exhaust Valve Opening (EVO) | [ <i>CAD</i> ] | 120    |
| Exhaust Valve Closure (EVC) | [ <i>CAD</i> ] | -350   |

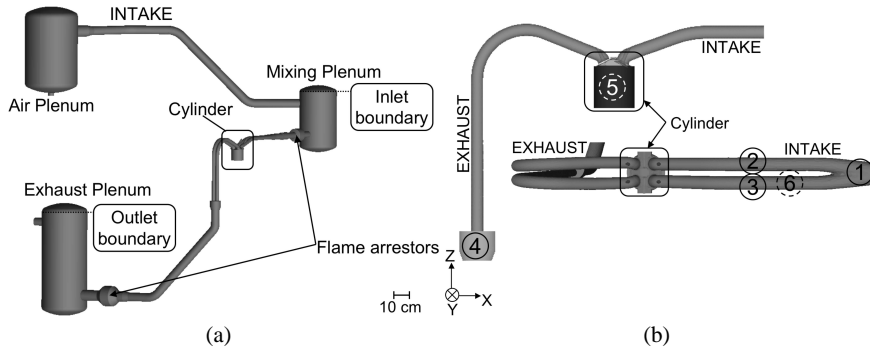


**Fig. 1** (a) Sketch of the experimental SGEmac engine test bench and locations of the LES boundaries. (b) Location of the experimental measurements: (1,2,3,4) pressure transducers; (5) PIV measurement in a vertical cross-section of the combustion chamber; (6) PIV measurement in a vertical cross-section of one of the intake ports.

The operating points acquired on this bench are documented in [24]. For fired points, the test bench is fueled with gaseous propane while for the non-reactive point the engine is only filled with air. Air and propane flow rates are controlled by sonic nozzles. Air is introduced in a tranquilization plenum and propane is then added in a mixing plenum. At the engine exhaust, gases are tranquilized in a third plenum. Since the engine is operated in a fully premixed mode, a flame-arrestor is added for safety reasons before each plenum (Fig. 1(a)). One hundred experimental consecutive cycles were acquired for each operating point.

Figure 1(b) shows the location of the various experimental acquisitions. PIV measurements are performed through a quartz cylinder and an optically transparent intake duct (planes 5 and 6) providing instantaneous and phase-averaged velocity fields. Several pressure transducers are used to record at one *CAD* resolution the pressure evolution along the intake (noted 1, 2 and 3) and exhaust ducts (noted 4).

In the literature, different parameters are used to quantify CCV. Variations in Indicated Mean Effective Pressure (IMEP) or in-cylinder peak pressure  $P_{max}$  are the most usual indicators of CCV [33,47]. For the present motored engine case (no

combustion), IMEP is not a relevant parameter and thus the variations can only be characterized with the in-cylinder flow field and  $P_{max}$ . Experimental measurements have shown that this operating point is very stable in terms of  $P_{max}$  with relative variations of about 1%.

### 3 LES of piston engines flows

LES is performed with a fully compressible Navier-Stokes solver on unstructured grids with a cell-vertex finite-volume formulation [31,39,16,17]. Centered spatial schemes and explicit time-advancement are used to control numerical dissipation and capture acoustics. For the present case, a Lax-Wendroff scheme [25], 2nd order in space and time, is employed with a time step conditioned by the acoustic CFL number.

The LES solver takes into account changes of heat capacity with temperature and composition using tabulated values of heat capacity for each species. The multi-species fluid follows the ideal gas law,  $P = \rho r T$  where  $P$  is the pressure,  $\rho$  is the density,  $T$  is the temperature and  $r$  is the mixture gas constant. Viscous transport terms are handled using classical gradient approaches. The fluid viscosity and the heat diffusion coefficient follow Sutherland's law and Fourier's law respectively. The species diffusion coefficients are obtained using a species Schmidt number along with Hirschfelder and Curtis approximation and velocity corrections for mass conservation [36].

Filtering the Navier-Stokes equations yields unresolved terms, which need to be modeled. The following closures of the subgrid scale (SGS) terms are used in the LES solver:

- The SGS stress tensor  $\overline{\tau}_{i,j}^t$  is closed using a Boussinesq approximation. This approximation introduces a turbulent viscosity  $\nu_T$  which is estimated with the standard Smagorinsky model [42] with a constant  $C_S = 0.18$ .
- The SGS species fluxes  $\overline{J}_i^k$  are modeled using a species SGS turbulent diffusivity  $D_k^t = \nu_T / Sc_k^t$ , where  $Sc_k^t$  is the turbulent Schmidt number ( $Sc_k^t = 0.6$  for all species  $k$ ).
- The SGS energy flux  $\overline{q}_i^t$  is modeled using the SGS turbulent thermal conductivity  $\lambda_{th}^t = \rho \nu_T C_p / Pr^t$  with  $C_p$  the heat capacity at constant pressure of the mixture and  $Pr^t$  the turbulent Prandtl number ( $Pr^t = 0.6$ ).

The methodology of Cook and Cabot [8] is used to treat shocks by introducing a hyper-viscosity in the viscous stress tensor which thickens the shock front. Such shocks can appear at moments where exhaust valves are opened.

The boundary condition treatment is based on a multi-species extension [31] of the Navier-Stokes Characteristic Boundary Conditions (NSCBC) [35].

### 4 Numerical Setup

Acoustics are a potential source of CCV and must be captured by LES. In the project SGEmac, two methodologies are explored [24]. The first considers the coupling of a system simulation (1D) and LES (3D), where the 3D simulation is

---

only applied on the combustion chamber and a part of the intake and exhaust pipes. The present scope of this paper concerns the second methodology which consists in applying LES on most of the experimental setup. Figure 1(a) shows the computational domain. The computed intake line extends from the mixing plenum to the cylinder while the exhaust line is fully computed. The two flame-arrestors are accounted for. The air plenum and the line between the two intake plenums have been removed since it is expected that most of the acoustic activity takes place between the cylinder and the mixing plenum. This configuration allows a simple and unambiguous definition of the boundary conditions (two plenum conditions). The following subsections detail the key points of the methodology used in this work.

#### 4.1 Mesh management

The whole computation domain is meshed using tetrahedra: it covers about 2.5 *m* from the intake boundary condition to the exhaust boundary condition and includes two plenums of 20 *l* (intake) and 50 *l* (exhaust).

In the present study, an engine cycle is divided into 41 phases (i.e. 41 grids) in order to maintain the quality of the mesh throughout the cycle. Between two computation phases, a second-order interpolation is used. The grids of each phase are generated before the simulation using a two-staged smoothing approach (Laplacian and optimization-based smoothing) [12]. As a reference, recent and comparable LES of IC engine used 20 phases with hexahedral-based grids [37,46] and 35 phases with hybrid tetrahedral/prismatic-based grids [19]. This method allows to avoid distortions of tetrahedra and to preserve accuracy and stability [46].

The smallest mesh contains 2.2 million cells at top-dead-center (TDC) while 9.6 million cells are required for the biggest mesh at bottom-dead-center (BDC). The characteristic cell size into the cylinder is of the order of 0.8 *mm*. The meshes are specifically refined around the valve seats, with a minimum of seven cells within a residual valve lift of approximately 0.35 *mm*. From the intake/exhaust ports to the plenums, the meshes are gradually derefined with a biggest characteristic cell size in the plenums of about 20 *mm*. Note that meshes are not refined at the walls since a law-of-the-wall formulation is used [39]. Figure 2 shows an overview of a typical tetrahedral mesh during the intake stroke.

#### 4.2 Boundary conditions

At the top of the intake and exhaust plenums, a pressure imposed boundary condition is set. The target pressures are not constant but time-varying plenum signals extracted from the experimental data which change between  $4.35 \times 10^4$  and  $4.5 \times 10^4$  *Pa* for the inlet plenum and  $9.9 \times 10^4$  to  $1.019 \times 10^5$  *Pa* for the outlet plenum. These signals are quasi sinusoidal with a frequency dictated by the engine rotational speed. As mentioned in the introduction, usual IC engine simulations consider boundary conditions directly in the ducts, close to the cylinder. Compared to a plenum signal, signals measured in the ducts (i.e. closer to the cylinder) vary much more and contain a wider spectrum of scales with many high frequencies: including the exhaust and intake ducts and imposing pressure in the

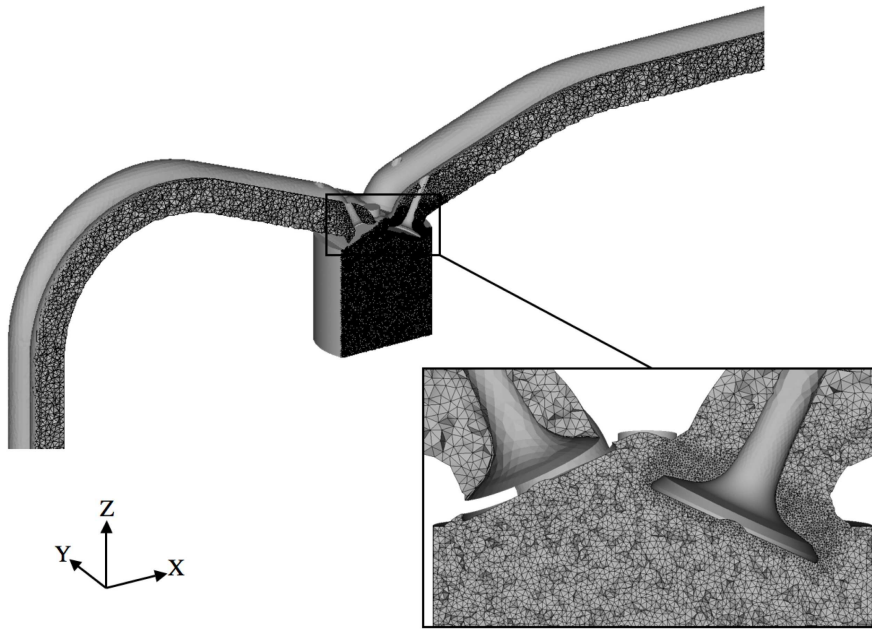


**Fig. 2** View of a typical tetrahedral mesh during the intake stroke.

plenums is obviously making the simulation easier.

Now, even if a larger computational domain makes the simulation simpler, it does not solve all boundary condition problems because acoustic impedances at inlets and outlets must be controlled: a section where pressure is strictly imposed is fully reflective for acoustic waves propagating in the LES while it is not necessarily so in the experiment. There is no easy solution to this difficulty. The best one is to locate boundary conditions as far as possible from the engine in places where pressure is really constant. Here, quasi nonreflective NSCBC are used via a Linear Relaxation Method (LRM) [38, 35] to impose pressure in the two plenums. LRM boundary conditions are well known to act as first order low-pass filters introducing a cut-off frequency that separates waves that will be reflected from the ones that will leave the domain [40]. This cut-off frequency is directly proportional to the relaxation coefficient imposed on the target pressure signal. Thus, one of the main advantages of a plenum boundary condition compared to a duct boundary condition is to allow the use of lower relaxation coefficients since the imposed signal varies much less and contains lower frequencies. As a consequence, the plenum boundary condition will be acoustically less reflective.

However, the introduction of a low relaxation coefficient can deteriorate the target signal, both in magnitude and in phase. In other words, the pressure signal which is actually recovered in the computation may differ from the target signal imposed in the plenums. For the range of relaxation coefficients used in this study, preliminary tests have shown that the LRM induces a negligible damping in magnitude. However, it leads to a phase shift between the target pressure (measured experimentally) and the inlet pressure obtained in the LES. This problem can be

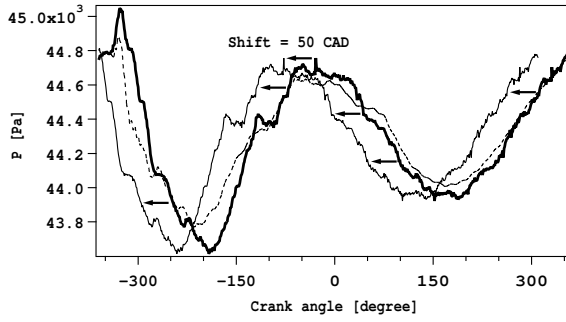


**Fig. 3** Pressure signals at the intake boundary condition. Experimental signal ( $\longrightarrow$ ), shifted target signal imposed in the computation ( $\longrightarrow$ ), signal recovered after imposition of the quasi non-reflective NSCBC ( $-\cdot-\cdot-$ ).

solved by shifting the target pressure in time as follows: for a signal composed of a single frequency  $f$ , Selle *et al.* [40] have demonstrated that the phase shift  $\Phi$  introduced by the reflexion coefficient  $\mathbf{A}$  of a characteristic boundary condition with a relaxation coefficient  $K$  can be estimated by:

$$\Phi = \arctan\left(\frac{\text{Im}(\mathbf{A})}{\text{Re}(\mathbf{A})}\right) \text{ with } \mathbf{A} = -\frac{1}{1 - i\frac{2\pi f}{K}} \quad (1)$$

Knowing  $\Phi$ , it is then possible to deduce the corresponding temporal shift  $\Delta t$  to impose on the initial target signal in order to obtain, after application of the LRM, the right desired signal:

$$\Delta t = \Phi / (2\pi f) \quad (2)$$

A similar methodology was extended to the multi-frequency pressure signals of the intake and exhaust boundary conditions. Figure 3 presents the results for the intake boundary condition. In this case, the shift induced by the relaxation coefficient (Eqs. 1 and 2) is evaluated to  $-0.0417$  s i.e.  $-50$  CAD. The experimental pressure signal has then been shifted by  $-50$  CAD and specified as target signal in the computation. The resulting inlet pressure in the LES, after applying boundary condition corrections, matches the experimental signal correctly. Thus this methodology allows to obtain acoustically well-defined boundary conditions while preventing any drift of the imposed signal. In addition, this boundary condition can take into account the acoustics in the ducts which is a possible source of CCV.

### 4.3 Modeling of the flame-arrestors

The flame-arrestors were introduced in the experiment for obvious security reasons, but from the computational point of view they represent an additional difficulty. Preliminary experimental studies of the flame-arrestor have been performed on an acoustic test bench [45]. They have shown that acoustic in the ducts is strongly perturbed by the presence of these flame-arrestors indicating that they



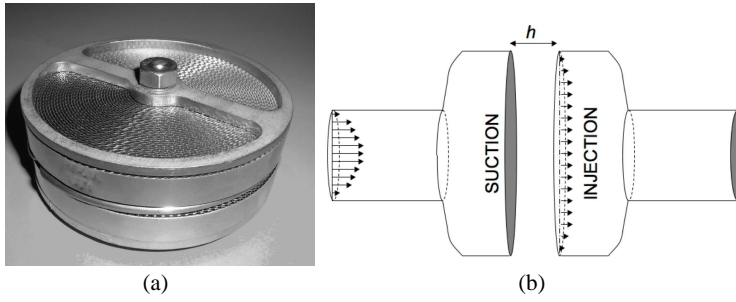


**Fig. 4** Flame-arrestor: (a) in the experiment; (b) in the computation.

must be included in the numerical setup. The flame-arrestors are spiral wound corrugated metal sheets which result in several hundred channels of diameter  $d = 0.5 \text{ mm}$  (Fig. 4(a)). Obviously such holes cannot be meshed. The solution adopted in this work is to model the flame-arrestor by two disjoint domains linked by a coupled suction/injection boundary condition (Fig. 4(b)). The equivalent flame-arrestor is characterized by a thickness  $h = 20 \text{ mm}$  (the distance between the two coupled boundary conditions) and a porosity  $\sigma = 0.68$ . The pressure drop  $\Delta P$  in the device is then given by the discharge law equation proposed by Mendez and Eldredge [28] originally developed for multi-perforated plates typically found in aeronautical combustion chambers. This model includes a time dependence to the mass flow rate which allows the condition to properly reproduce the acoustic properties of the holes:

$$\Delta P = \frac{\rho l'}{\sigma \sin(\alpha)} \frac{\partial U_W}{\partial t} + \frac{1}{2C_D^2} \rho \frac{U_W^2}{\sigma^2 \sin^2(\alpha)} \quad (3)$$

where  $l' = \frac{\pi d}{4} + h$  is a characteristic length determined to match the Howe model [10],  $U_W$  is the bulk velocity and  $\alpha$  is the inclination angle of the aperture. In this expression, the discharge coefficient  $C_D$  depends on the bulk velocity  $U_W$  (given by the manufacturer).

## 5 Results and Discussion

The whole simulation covers 27 consecutive cycles. Computation starts at IVO with a flow at rest. The turnaround time of a single LES cycle is about 18 hours on 400 processors of a SGI Altix ICE 8200 cluster. Figure 5 presents the evolution of the trapped mass for the 27 consecutive LES cycles. The first two cycles are strongly influenced by the initialization of the simulation and are discarded in the following analysis. Thus, 25 cycles remain for the comparison with the experimental data. The 25 remaining LES cycles are very stable in terms of trapped mass around  $200.6 \text{ mg}$ . The difference compared to the value estimated in the experiment ( $199.9 \text{ mg}$ ) is approximately 0.5%.

The validation of the multi-cycle LES is organized as follows:

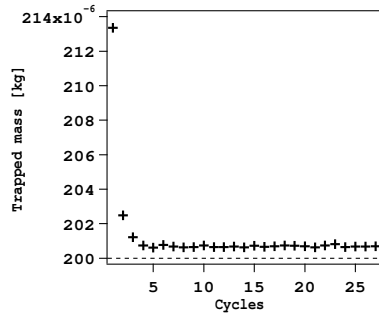


**Fig. 5** Evolution of the trapped mass in the cylinder for the 27 LES cycles. The experimental trapped mass (---) is estimated to 199.9 mg.

- First, the flow field activity in the ducts is validated using PIV measurements (plane 6 in Fig. 1(b)) and temporal pressure acquisitions (probes 1 and 4 in Fig. 1(b)) in the intake and exhaust manifolds. Acoustic wave propagation in the intake and exhaust ducts is specifically investigated.
- Second, the LES quality inside the cylinder is assessed and the flow behavior is compared to the experimental data in terms of in-cylinder pressure and aerodynamic field throughout the cycle. CCV are highlighted and analyzed.

### 5.1 Flow behavior in the intake and exhaust ducts

Figure 6 shows the pressure evolution during the whole cycle at the intake and exhaust manifolds (probes 1 and 4 respectively in Fig 1(b)) and the good agreement between phase-averaged LES and experimental signals. The two signals exhibit the same progressive damping when the valves are closed (between IVC and IVO for the intake duct and between EVC and EVO for the exhaust duct, see Table 1). The fact that LES and experimental signals match very well during the whole cycle shows that the modeling described in Section 4.3 is able to reproduce the right impedance of the flame-arrestors. The signal extracted from a simulation without flame-arrestor (also reported in Fig. 6 (right) for the exhaust line) shows that the main effect of the flame-arrestor is to damp the oscillations, the phase of the signal being little affected. The same behavior may be observed for the intake line. Despite this satisfactory global behavior, the LES signal in the intake duct shows a superimposed high frequency signal around 430 Hz which is not present in the measurements.

To determine the nature of the 430 Hz frequency appearing in the LES pressure signal, two diagnostics were used: a spectral analysis of the LES results via a spectral map and an acoustic analysis of the configuration via a Helmholtz solver. The spectral map consists in FFT analysis applied on multiple pressure probes recorded on the centerline of the intake duct. The sample frequency of the pressure signals is 100 kHz and the spectral resolution of the FFTs is 0.4 Hz since 25 LES cycles are recorded corresponding to a total physical time of 2.5 s. The spectral map of the LES pressure signals reveals a very wide spectrum with many characteristic frequencies, going (for the most energetic ones) from 10 Hz, the

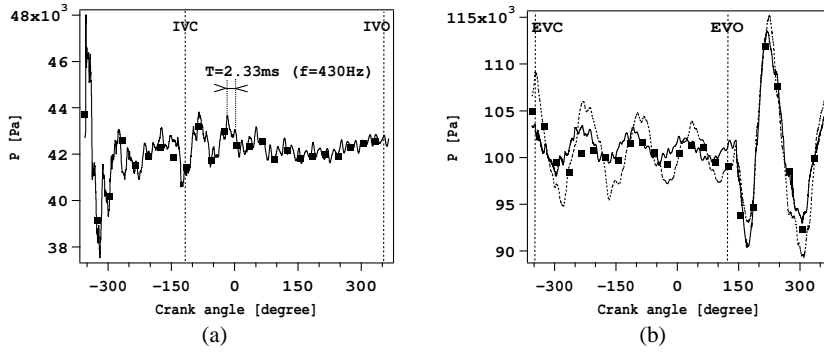


**Fig. 6** Phase-averaged mean pressure in the intake (a) and exhaust (b) manifolds, measurement noted 1 and 4 respectively in Fig. 1(b). LES:—; experiments: ■. LES results without modeling of the flame-arrestors (- - -) are also shown for the exhaust manifold.

**Table 2** Longitudinal mode frequencies predicted by the Helmholtz solver and by the LES for the intake line.

| Mode number | name     | location                | Frequency [Hz]   |     |
|-------------|----------|-------------------------|------------------|-----|
|             |          |                         | Helmholtz solver | LES |
| 1           | 1/4 wave | full intake line        | 108              | 110 |
| 2           | 1/4 wave | from valves to manifold | 234              | -   |
| 3           | 3/4 wave | full intake line        | 251              | 250 |
| 4           | 5/4 wave | full intake line        | 405              | 430 |

frequency of the valve opening, to 630 Hz. The structure of the 430 Hz mode is shown in Fig. 7 (top). This mode is an acoustic eigenmode of the intake duct and this can be checked by using an acoustic Helmholtz solver [32]. This code (called AVSP) solves the eigenvalue problem associated to the Helmholtz equation which solves the wave equation in a flow:

$$\nabla \cdot (c^2 \nabla \hat{p}) + \omega^2 \hat{p} = 0 \quad (4)$$

where  $c$  is the local speed of sound and  $\hat{p}$  is the Fourier transform of the pressure fluctuations at the radial frequency  $\omega = 2\pi f$ . This solver has been applied to the intake line with the valves closed since AVSP is not able to take into account moving boundaries. The results in Table 2 show that four main longitudinal acoustic modes coexist in the intake line. The modes 1, 3 and 4 are respectively the quarter wave, three-quarter wave and five-quarter wave modes of the full line. The mode 2 is the quarter wave mode between the valves and the intake manifold and it is damped in the LES. The analysis of the spatial structure of the five-quarter wave mode at 405 Hz (Fig. 7 bottom) shows that the correspondence with the 430 Hz mode found in the LES is excellent. The slight shift of frequency and of spatial structure is certainly due to the fact that the spectral map is built over the whole cycle, i.e. valves opened and closed, contrary to the acoustic configuration. This result confirms that this 430 Hz LES mode is a real mode of acoustic nature and not a hydrodynamic effect or a numerical artifact. Of course, the AVSP result

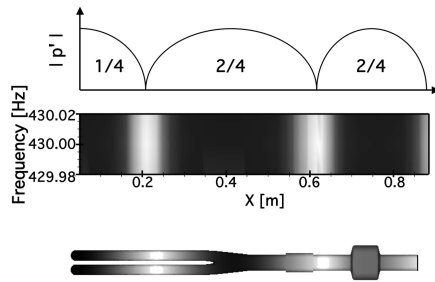


**Fig. 7** Spatial structure of the five-quarter wave longitudinal mode in the intake ducts. Comparison of the field of  $|p'|$  between spectral map on the duct axis (top) and the Helmholtz solver results in the whole intake domain (bottom).

cannot explain why this acoustic mode is damped in the experiment and not in the computation. Experimental measurements made without flame-arrestors have shown that they are not the source of damping. This point must still be explored but the agreement between LES and experiment in Fig. 6 remains excellent anyway.

Figure 8 compares the phase-averaged crank-resolved pressure obtained in the LES to the experimental measurements at probe 3. The corresponding phase-averaged axial velocity is also shown. Experimental velocity values are extracted from PIV measurements on the centerline of the duct. Negative velocities indicate a fluid flowing from the plenum to the cylinder. LES and experiments are in good agreement during the whole cycle, both for the pressure and the velocity. The strong back-flow occurring at IVO ( $CA = -360^\circ$ ) is clearly visible. This phenomenon is not localized close to the cylinder only. During about 20 CAD the complete intake line flows back to the plenum. Thereafter, the flow enters the cylinder until a second minor back-flow occurs again just before IVC ( $CA = -170^\circ$ ). When the valves are closed at  $CA = -120^\circ$ , the flow continues to oscillate between the intake ports and the plenum. The variations from one cycle to another are roughly constant during the whole cycle, of the order of  $\pm 2$  m/s. It is worth reminding that this behavior corresponds to a probe located on the centerline of the duct. A probe located at the same longitudinal position but shifted in the radial direction exhibits noticeably different evolution. In extreme cases, both positive and negative velocities may be found in a given section of the duct as shown in Fig. 9. This complex evolution of the velocity, rapidly varying from negative to positive values both in space and in time, confirms how challenging it would be to set a boundary condition in section 3 (Fig. 1(a)) because it is too close to the engine. At this section, the flow changes sign with time and is not homogeneous in space. Considering Fig. 9, the simple question of defining if the boundary condition should be an inlet or an outlet is already a difficult task. Moreover, it has to be noted that all hot gases flowing back to the intake boundary condition are "lost" for the computation since the boundary condition is generally built only to feed cold fresh gases into the domain. This is not very problematic for a motored engine computation where all gases have a quasi constant composition and temperature but it may become

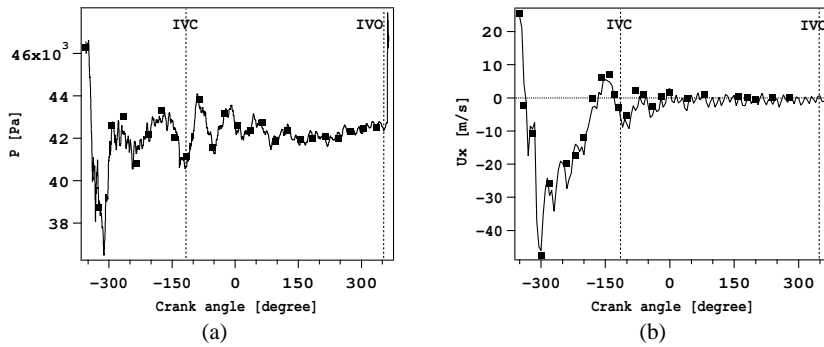


**Fig. 8** Phase-averaged crank-resolved pressure (a) and velocity (b) in the intake duct, measurements noted 3 and 6 respectively in Fig. 1(b). LES:—; experiments: ■.

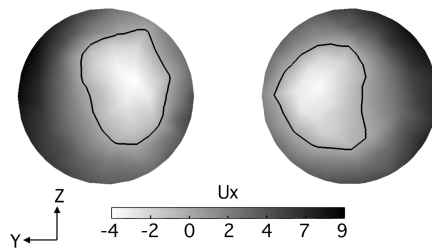


**Fig. 9** Phase-averaged axial velocity field (LES) in a cutting plane through the intake ducts at 180 CAD before TDC (location 3 in Fig. 1(b)). The isoline of null velocity is also plotted.

an important source of errors for reacting cases where gases leaving the engine strongly differ from fresh gases feeding it.

## 5.2 In-cylinder predictions

### Flow characteristics

Figure 10 shows instantaneous velocity fields obtained by LES at four distinct times. These fields exhibit the typical structures encountered during the intake, compression and exhaust strokes. At IVO, a back-flow first occurs due to the lower pressure within the intake pipe. Then, after about 20 CAD, fresh gases start entering the cylinder. The annular valve jets interact with the cylinder head and the piston to form smaller structures (Fig. 10(a)). At higher valve lifts (Fig. 10(b)), the jet direction coupled to the piston movement induces a well-known tumbling motion in the cylinder. During compression, the tumble motion becomes more and more structured until TDC as illustrated in Fig. 10(c). This organized motion disappears during the expansion stroke. The exhaust stroke also begins with a back-flow from the exhaust pipe into the cylinder. Due to the very small valve lift, the flow is sonic around the valve heads (Fig. 10(d)). At higher exhaust valve lifts, the pressures of the exhaust pipes and the cylinder balance out and air is driven

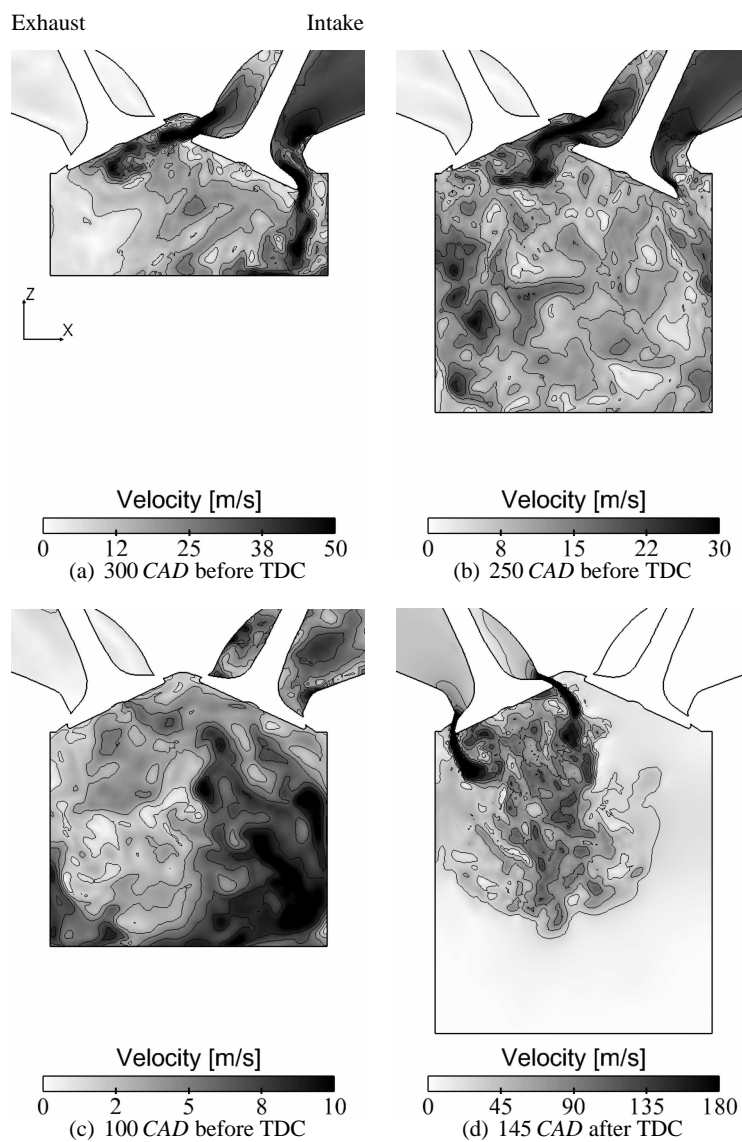


**Fig. 10** Instantaneous velocity fields (LES) in a vertical cross-section of the 10th cycle.

out by the piston motion.

The evolution of the in-cylinder pressure during the whole cycle is plotted in Fig. 11. Both mean LES cycle and mean experimental cycles are depicted. During the main part of the cycle (Fig. 11(a) and Fig. 11(c)), the mean LES signal is superimposed to the experimental curve. However, during the compression stroke (Fig. 11(b)) LES overpredicts the pressure rise, leading to a higher maximum mean pressure. Afterwards, the LES recovers the experimental curve with a very

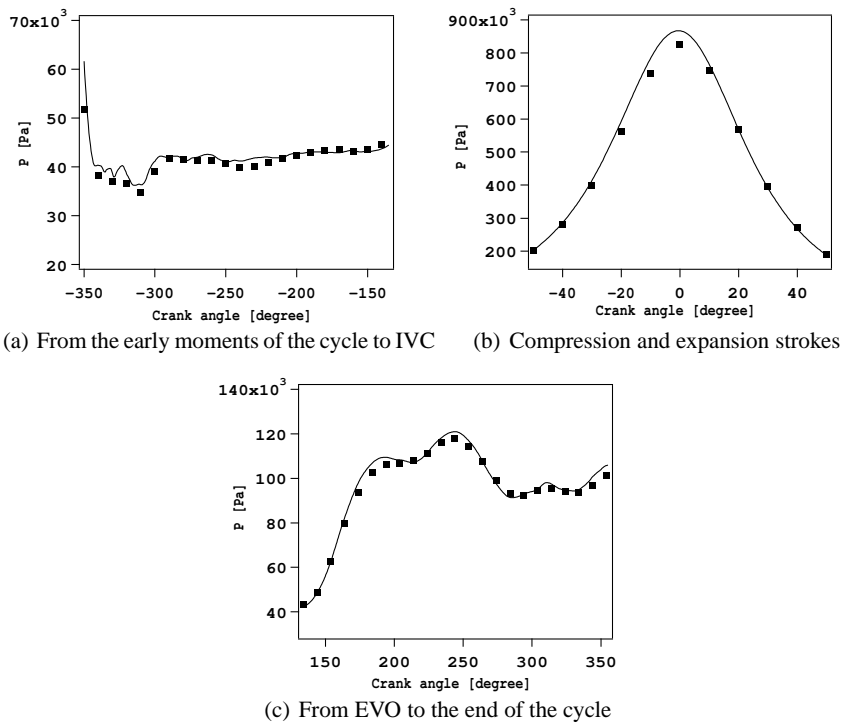


**Fig. 11** Evolution of experimental (■) and LES (—) phase-averaged cylinder pressure during the whole cycle.

good agreement. The LES behavior around TDC indicates that the compression ratio used in the simulation differs from the experimental one, certainly because of blowby issues often encountered experimentally with optical engines.

#### Assessment of quality and reliability of the multi-cycle LES

Before going into more details, the quality and the reliability of the multi-cycle LES has to be assessed. The quality of a LES may be investigated using two categories of estimators: single-computation estimators or grid-model procedures which require several simulations (typically a standard simulation, then a simulation with a modified SGS model, and finally a coarse grid simulation) [22,6,23]. In the present study, the efforts in terms of grid meshing and CPU time are too important for considering the second class of indicators. Therefore the quality of the simulation is evaluated by means of the ratio between SGS viscosity  $\nu_T$  and fluid viscosity  $\nu$ . Figure 12 displays the evolution of the mean and maximum ratio over the cylinder volume. The mean values are globally low ( $< 6$ ) during the whole cycle whereas the maximum values do not exceed 20. These results indicate that the set of grids used in the simulation allows a correct resolution of the flow during

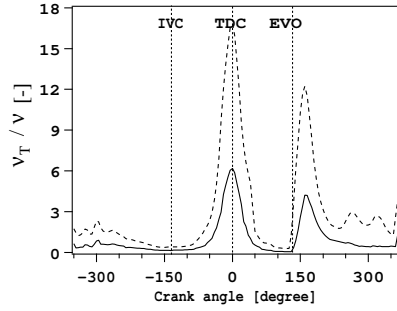


**Fig. 12** Computed SGS viscosity normalized by fluid viscosity in the cylinder: volume-averaged ratio (—), maximum ratio (---).

most of the cycle. The most critical periods in terms of flow resolution are encountered around compression TDC and EVO. Indeed, during the compression stroke, the grid resolution stays almost constant (from  $0.8\text{ mm}$  at BDC to  $0.65\text{ mm}$  at TDC) while the turbulent scales strongly decrease (typically by a factor of ten [21, 7]), leading to an insufficient resolution around TDC. At EVO, the grid is much more refined ( $\sim 0.07\text{ mm}$  in the valve seats) but the turbulent activity generated by the high speed jets in the valve seats ( $\sim 480\text{ m/s}$ ) is too strong to avoid higher levels of turbulent viscosity.

The reliability of the simulation is also controlled by the statistical sampling. In order to compare the LES to the experiments, phase averaging is performed: phase-averaged quantities are obtained using 25 cycles in the LES and 100 cycles in the experiment. Previous studies [30, 9, 44, 18] have already addressed the impact of the number of cycles used for phase averaging. For gauging the relevance of the LES sample size, a convergence analysis was performed first on the experimental data. It consists in evaluating the difference between a phase-averaged velocity over  $n$  cycles ( $n = 10, 25, 50, 75$ ) and the reference phase-averaged velocity over 100 cycles. The difference  $\epsilon_n^{CA}$  evaluated by Eq. 5 is computed along a vertical velocity profile sketched in Fig. 16(a):

$$\epsilon_n^{CA} = \frac{1}{\Delta z} \int_{piston}^{cylinder\ head} \left| \frac{\langle \sqrt{U_x^2 + U_z^2} \rangle_n^{CA} - \langle \sqrt{U_x^2 + U_z^2} \rangle_{100}^{CA}}{\langle \sqrt{U_x^2 + U_z^2} \rangle_{100}^{CA}} \right| dz, \quad (5)$$

where  $\langle \cdot \rangle_n^{CA}$  is the ensemble averaging over  $n$  cycles at a given crank angle  $CA$  and  $\Delta z$  is the integration vertical height.

Table 3 shows the error  $\epsilon_n^{CA}$  at four instants of the intake and compression strokes. It suggests that  $n = 25$  is sufficient to evaluate the mean in-cylinder dynamics since the experiment shows a difference of about 6% between a phase-averaging over 25 cycles and a phase-averaging over 100 cycles. A similar study was carried out for the root mean square (RMS) of the velocity. Table 3 indicates that a minimum of 50 cycles would be necessary to obtain an error of 10% on RMS velocities, thus confirming the hypothesis of Heywood [21] or Celik *et al.* [4] for example. It is worth noting that 25 cycles allow an acceptable estimate of the RMS values nonetheless ( $\sim 10\%$  error except in the early times after valve opening).



**Table 3** Convergence analysis on the number of experimental cycles used for ensemble averaging: differences with respect to reference quantities averaged over 100 cycles.

| <i>CAD before</i> | <b>Mean velocity</b> |                      |                      |                      | <b>RMS of velocity</b> |                      |                      |                      |
|-------------------|----------------------|----------------------|----------------------|----------------------|------------------------|----------------------|----------------------|----------------------|
|                   | $\epsilon_{10}$<br>% | $\epsilon_{25}$<br>% | $\epsilon_{50}$<br>% | $\epsilon_{75}$<br>% | $\epsilon_{10}$<br>%   | $\epsilon_{25}$<br>% | $\epsilon_{50}$<br>% | $\epsilon_{75}$<br>% |
| <b>TDC</b>        |                      |                      |                      |                      |                        |                      |                      |                      |
| 280               | 9.7                  | 5.5                  | 3.9                  | 3                    | 22.4                   | 17.7                 | 11.4                 | 5.2                  |
| 240               | 8.4                  | 6.2                  | 2.3                  | 1.7                  | 16.4                   | 9.3                  | 5.2                  | 1.9                  |
| 180               | 15                   | 6.4                  | 4.7                  | 2.3                  | 19.9                   | 9.7                  | 7.1                  | 4.4                  |
| 100               | 17                   | 5.6                  | 3.6                  | 1.3                  | 20                     | 12                   | 7                    | 2.3                  |

**Table 4** Convergence analysis on the number of LES cycles used for ensemble averaging: differences with respect to reference quantities averaged over 25 cycles.

| <i>CAD before</i> | <b>Mean velocity</b> |                      |                      |                      | <b>RMS of velocity</b> |                      |                      |                      |
|-------------------|----------------------|----------------------|----------------------|----------------------|------------------------|----------------------|----------------------|----------------------|
|                   | $\epsilon_5$<br>%    | $\epsilon_{10}$<br>% | $\epsilon_{15}$<br>% | $\epsilon_{20}$<br>% | $\epsilon_5$<br>%      | $\epsilon_{10}$<br>% | $\epsilon_{15}$<br>% | $\epsilon_{20}$<br>% |
| <b>TDC</b>        |                      |                      |                      |                      |                        |                      |                      |                      |
| 280               | 23.4                 | 13.8                 | 6.5                  | 3.5                  | 47.4                   | 24.2                 | 13.2                 | 6.9                  |
| 240               | 17.5                 | 7.4                  | 5.2                  | 2.2                  | 38.8                   | 20.5                 | 11.4                 | 5.3                  |
| 180               | 13.3                 | 6.1                  | 5                    | 4.3                  | 49.1                   | 17.5                 | 8.5                  | 8.1                  |
| 100               | 9.6                  | 6.4                  | 5.1                  | 3.7                  | 58.4                   | 26.1                 | 12.7                 | 6.5                  |

The same analysis can be then done for LES results but only on 25 cycles. Table 4 shows that computing 10 cycles only (as done by several authors [9, 46, 19]) allows a reasonable analysis of the mean flow. Conversely and as expected, this is insufficient for RMS quantities considering that the reference values obtained with 25 cycles are already a limited estimation of the real values.

It has to be mentioned that this analysis is of course restricted to an aerodynamic point of view since the configuration is a motored engine case. For fired operating points, the same kind of analysis could be carried out with combustion indicators like the flame surface or heat release fields. If the same conclusions are probably valid for stable and weakly unstable operating points, one can expect a noticeably different conclusion for highly unstable cases. (i.e. a much larger statistical sampling would be necessary).

#### In-cylinder flow field

Figures 13 and 14 compare the measured data to the computed phase-averaged axial and vertical velocity fields in the median plane of the cylinder (plane 5 in Fig. 1(b)) at four distinct times. The axial velocity fields are more representative of the flow motion induced by the valves whereas the vertical component is more representative of the movement of the piston. Note that the window of PIV measurement (Fig.1(b)) has been reduced to exclude zones where laser reflections or leaking oil issues were encountered in the near wall region. In the remaining window, the LES mean axial velocity component is in good agreement with the experimental data. The global shape and the level of velocities measured by PIV

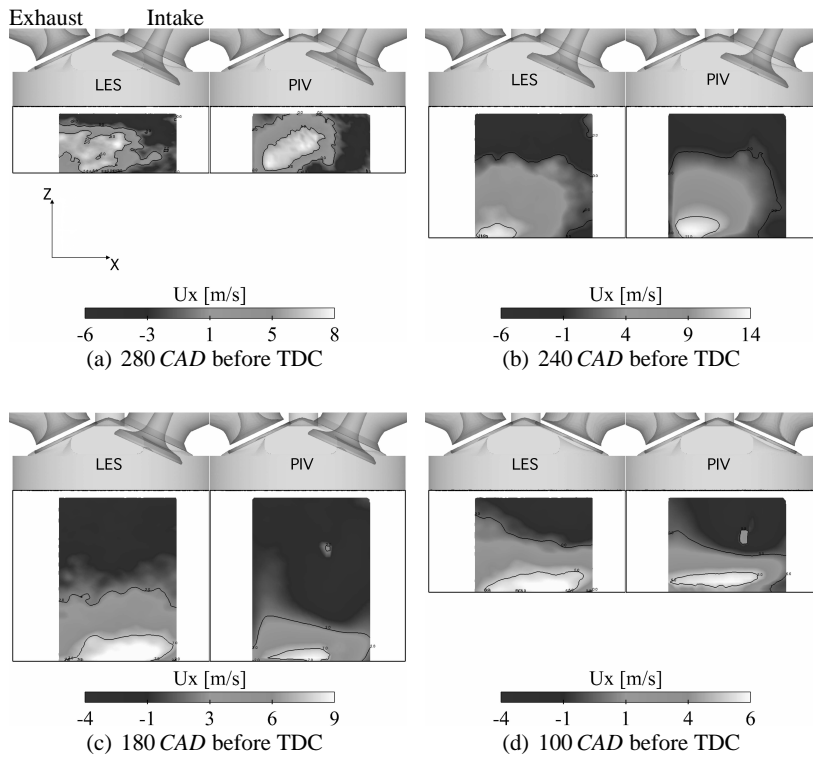


**Fig. 13** Comparison of LES (left) and PIV (right) results for the phase-averaged axial velocity component (measurement noted 5 in Fig. 1(b)) at four instants.

are well reproduced by LES. Nevertheless, discrepancies are observed, especially at 280 *CAD* before TDC. For the mean vertical velocity component, the discrepancies are slightly larger. On the right side of the chamber, the valve jet does not penetrate in the LES as far as in the experiment (Figs. 14(b) and 14(c)), resulting in a different jet/tumble interaction in the upper part of the chamber. However, the overall comparison of the flow structure remains rather good.

### 5.3 Cycle-to-cycle analysis

In this section, the emphasis is put on the CCV analysis of pressure and velocity variations in the cylinder: CCV are usually studied in terms of maximum cylinder pressure but this quantity gives only a global overview of the engine stability. The study of velocity CCV allows a more precise and local characterization of the flow unsteadiness.

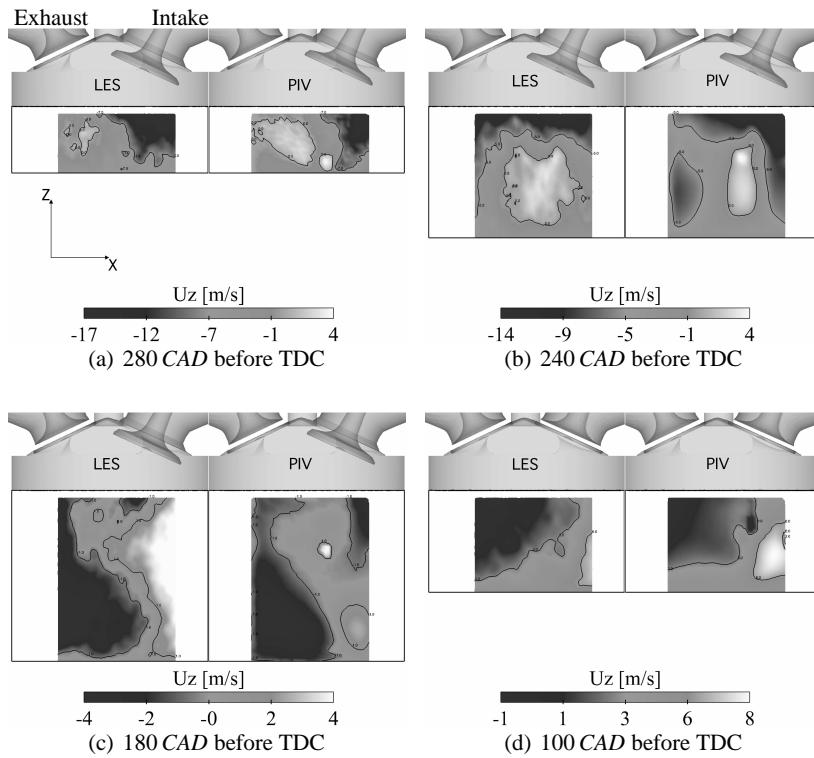


**Fig. 14** Comparison of LES (left) and PIV (right) results for the phase-averaged vertical velocity component (measurement noted 5 in Fig. 1(b)) at four instants.

### Pressure variations

Figure 15 presents the return map of the maximum in-cylinder pressure. This consists in plotting the maximum pressure of cycle  $i + 1$  (normalized by the maximum pressure of the mean cycle) versus the maximum pressure of the preceding cycle  $i$ . The level of CCV in the cylinder pressure is very low for both LES and experiment (relative variation  $< 0.4\%$ ), meaning that LES correctly reproduces the stability of the experimental point. One can observe that neither LES nor experiment exhibit a regular pattern meaning that no obvious relation exists between a cycle and the following one. However, little less CCV are observed in the LES compared to the experiments. Contrary to the experiment where the pressure signal at the plenum slightly varies from cycle to cycle, the same signal is imposed in the LES for all cycles. Tests are currently underway to check if this simplification could modify the results in terms of cyclic variations. The difference in sampling size could be another reason for these discrepancies. Finally, the use of a relatively low-order numerical scheme combined with a Smagorinsky model known to be dissipative may also lead to an excessive dissipation that could reduce CCV.

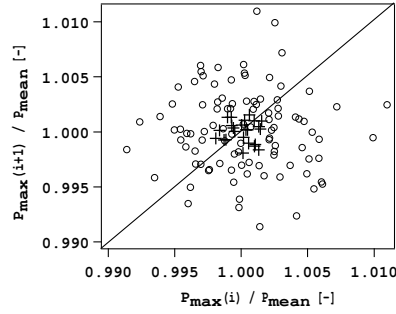


**Fig. 15** Maximum in-cylinder pressure of cycle  $i+1$  (normalized by the maximum in-cylinder pressure of the mean cycle) versus the maximum in-cylinder pressure of the preceding cycle  $i$ ; comparison between experimental ( $\circ$ ) and LES ( $+$ ) results.

### Aerodynamics variations

Even if pressure CCV are very low, CCV can be significant for the in-cylinder flow field. To illustrate this point, Fig. 16 shows CCV in the axial velocity at different crank angles. The axial velocity component is plotted along the  $z$ -axis in the center of the cylinder. For the sake of clarity, the 100 experimental cycles are not superimposed and only a confidence envelope is plotted. The lower and upper part of the confidence envelope contains 95% of the experimental cycles and are estimated as  $\langle U_x \rangle_{100} - 2 \cdot \sigma_{U_x}$  and  $\langle U_x \rangle_{100} + 2 \cdot \sigma_{U_x}$  respectively, with  $\sigma_{U_x}$  the standard deviation of the axial velocity.

Fig 16(b) shows that CCV levels are slightly higher in the upper region of the profiles during the first times of the intake stroke, due to valve jets. During compression, Fig. 16(d) and (e) show that the variations are homogeneous over the entire height of the chamber with lower levels than during the intake stroke. However, a normalization by the mean velocity reveals that the relative intensity of the variations is stronger during the compression stroke, as already shown by Goryntsev *et al.* [14]. The comparison between the computed instantaneous cycles and the confidence envelope is satisfactory during the whole cycle, especially during the intake stroke, meaning that LES is able to capture the variations of the in-cylinder dynamic.

To determine precisely where aerodynamic CCV occur during a cycle, a proper orthogonal decomposition (POD) [26] analysis of the in-cylinder velocity field is carried out using the snapshot method introduced by Sirovich [41]. To take into account the deformation during a cycle, a phase-dependent POD is performed every 5 CAD [11]. Figure 17 presents the energy distribution of the ten highest energy modes found in the POD as a function of the CA. The largest part of the energy ( $\sim 70\%$ ) is contained in the first mode which corresponds to the mean flow (similar results were found in [1]). The other modes reveal the velocity fluctuations and their corresponding energy denotes their level. In other words, at a considered CA, POD allows an energetic classification of the CCV of the in-cylinder dynamic. The ratio between energies of the first and second mode suggests that CCV are very low during the intake stroke ( $\sim 3\%$ ) and become stronger during the com-

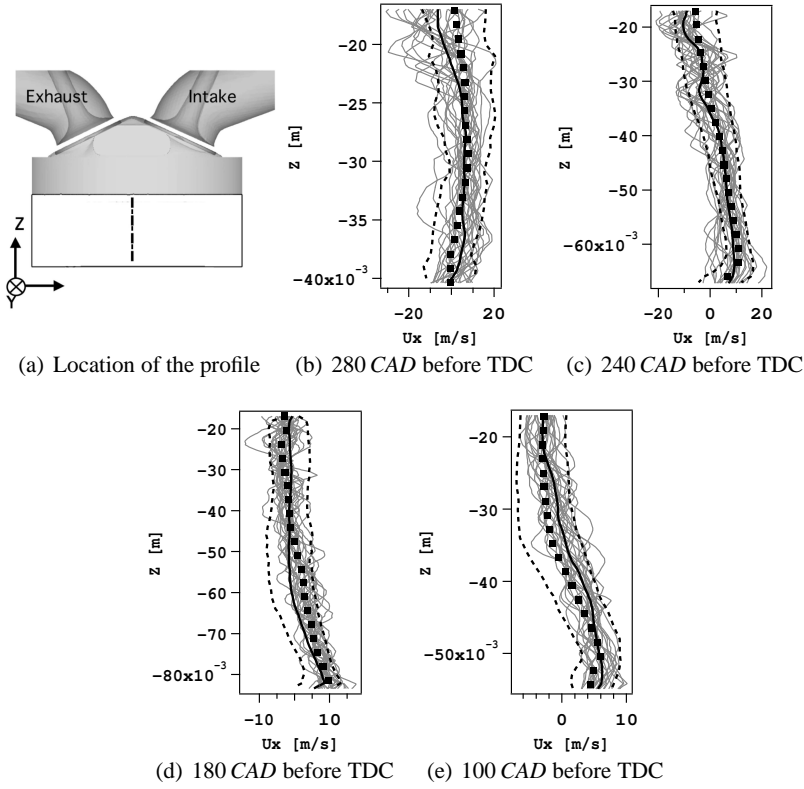


**Fig. 16** The dashed line in (a) represents the line along which all of the profiles are plotted. (b)-(e) Comparison of axial velocity profiles between the 25 instantaneous LES cycles (—), the mean LES (—), the mean experiment (■) and the 95% confidence envelope of the 100 instantaneous experimental cycles (---).

pression with a maximum value near TDC ( $\sim 9.5\%$ ) due to the vortex breakdown and near BDC of the expansion stroke ( $\sim 7.5\%$ ). This result is thus consistent with the previous analysis for velocity profiles.

Figure 18 presents iso-surfaces of the most and second most energetic POD modes found inside the cylinder. It shows that CCV at 280 CAD before TDC are mainly created in the mid-plane of the cylinder by the shear between the valve jets. Then the flapping of the jets becomes the main source of variation as illustrated in Fig. 18(b).

At 180 CAD before TDC, the location of the most energetic mode completely changes. Indeed, at this crank angle the tumbling motion becomes the most energetic mode instead of the intake jets. During the compression stroke, Fig. 18(d) shows that variations are provided by the wall/tumble interaction and some variations are also concentrated in the center of the cylinder, which may be related to a tumble core precession [27, 3].

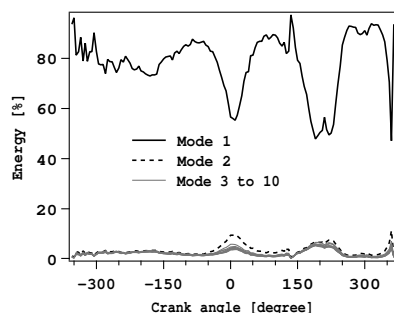
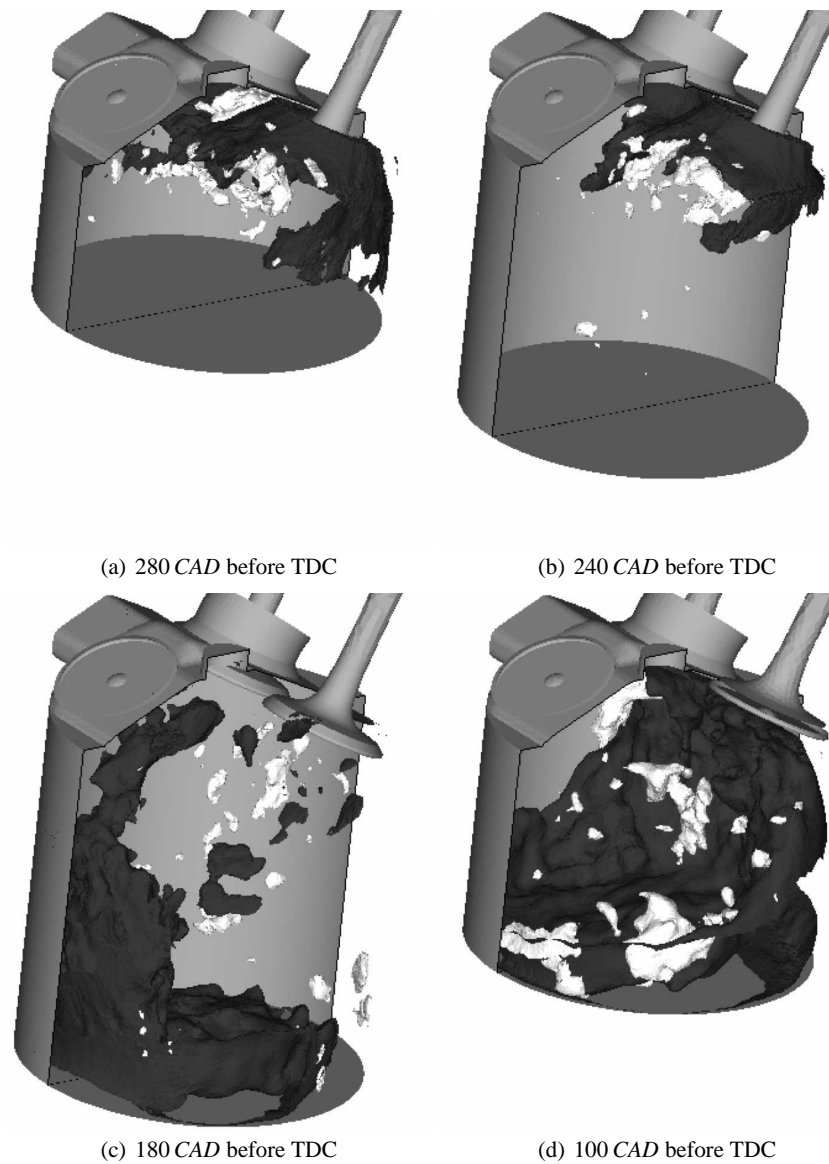


Fig. 17 Energy distribution of the first 10 most energetic POD modes.

## 6 Conclusion

This paper presents a methodology designed to study CCV (Cycle-to-Cycle Variations) in IC engines using multi-cycle LES. In order to limit the influence of the boundary conditions and to ensure proper acoustic resolution, the computational domain takes into account almost the whole experimental bench including intake and exhaust ducts and plenums. The numerical strategy includes mesh movement of tetrahedral elements, modeling of the flame-arrestors and specific treatments of boundary conditions at inlet and exhaust. The methodology is tested on a non-reacting stable operating point with low CCV and compared to experimental results. 27 consecutive LES cycles are computed but only 25 cycles are considered for the analysis. Very reasonable turnaround time is achieved since only 18 hours (elapsed time) are necessary to compute a single cycle. Acoustic activity in intake and exhaust ducts is validated against both pressure transducer measurements and a Helmholtz solver. The flow dynamic in the cylinder is well reproduced by LES with levels of CCV comparable to the experiments. The highest absolute variations are found during the intake stroke but a normalization by the mean flow reveals that the maximum relative variations rather occur during the compression stroke. This report is confirmed by a proper orthogonal decomposition analysis that spatially locates the dynamic variations and denotes their corresponding energy. The high levels of dynamic CCV have little impact on the evolution of the cylinder pressure. The variations in maximum pressure are indeed very low both in the LES and in the experiments. The stable nature of the operating point is thus well reproduced by the simulation. The next step is to apply this methodology for fired operating points with higher CCV levels. The ability of LES to predict both stable and unstable points and their corresponding CCV will be analyzed in future publications.

**Acknowledgements** The authors gratefully acknowledge the financial support provided by PSA Peugeot Citroën and Renault SAS in the framework of thesis researches. This work was granted access to the HPC resources of CINES (Centre Informatique National de l'Enseignement Supérieur) under the allocation 2009-c2009026055 made by GENCI (Grand Equipement National de Calcul Intensif). The authors also acknowledge the financial support by ANR (Agence Nationale de la Recherche) under grant N.ANR-06-PDIT-007-01 SGEmac.



**Fig. 18** Iso-surfaces of eigenfunctions of the POD first (black) and second (white) most energetic modes.

## References

1. Baby, X., Dupont, A., Ahmed, A., Deslandes, W., Charnay, G., Michard, M.: A new methodology to analyse cycle-to-cycle aerodynamic variations. SAE Paper (2002-01-2837) (2002)
2. Boileau, M., Staffelbach, G., Cuenot, B., Poinot, T., Bérat, C.: LES of an ignition sequence in a gas turbine engine. *Combust. Flame* **154**(1-2), 2–22 (2008)

3. Borée, J., Maurel, S., Bazile, R.: Disruption of a compressed vortex. *Phys. Fluids* **14**(7), 2543–2556 (2002)
4. Celik, I., Klein, M., Freitag, M., Janicka, J.: Assessment measures for URANS/DES/LES: an overview with applications. *J. Turb.* **7**(48), 1–27 (2006)
5. Celik, I., Yavuz, I., Smirnov, A.: Large eddy simulations of in-cylinder turbulence for internal combustion engines: a review. *Int. J. Engine Research* **2**(2), 119–148 (2001)
6. Celik, I.B., Cehreli, Z.N., Yavuz, I.: Index of resolution quality for large eddy simulations. *J. Fluids Eng.* **127**(5), 949–958 (2005)
7. Celik, I.B., Yavuz, I.: An assessment of turbulence scales relevant to internal combustion engines. *Internal Combustion Engine Division Spring Tech. Conf.* **28**(1), paper 97–ICE-5 (1997)
8. Cook, A.W., Cabot, W.H.: Hyperviscosity for shock-turbulence interactions. *J. Comput. Phys.* (2004)
9. Dugue, V., Gauchet, N., Veynante, D.: Applicability of large eddy simulation to the fluid mechanics in a real engine configuration by means of an industrial code. *SAE Paper* (2006-01-1194) (2006)
10. Eldredge, J.D., Bodony, D.J., Shoeybi, M.: Numerical investigation of the acoustic behavior of a multi-perforated liner. *aiaa paper* 2007-3683. In: 13th AIAA/CEAS Aeroacoustics Conference, Rome, 21–23 May 2007 (2007)
11. Fogleman, M., Lumley, J., Rempfer, D., Haworth, D.: Application of the proper orthogonal decomposition to datasets of internal combustion engine flows. *J. Turb.* **5**(023) (2004)
12. Forsythe, N., Müller, J.D.: Validation of a fluid-structure interaction model for a bileaflet mechanical heart valve. *Int. J. Comput. Fluid Dynamics* **22**(13), 541–553 (2008)
13. Fureby, C.: Towards the use of large eddy simulation in engineering. *Progress in Aerospace Sciences* **44**, 381–396 (2008)
14. Goryntsev, D., Klein, M., Sadiki, A., Janicka, J.: Large eddy simulation of fuel-air mixing in a direct injection SI engine. In: 5th Symp. on Turb. and Shear Flow Phenomena. Munich, Germany (2007)
15. Goryntsev, D., Sadiki, A., Klein, M., Janicka, J.: Large eddy simulation based analysis of the effects of cycle-to-cycle variations on air-fuel mixing in realistic DISI IC-engines. *Proc. Combust. Inst.* **32**, 2759–2766 (2009)
16. Gourdain, N., Gicquel, L., Montagnac, M., Vermorel, O., Gazaix, M., Staffelbach, G., García, M., Boussuge, J.F., Poinot, T.: High performance parallel computing of flows in complex geometries - part 1: methods. *Comput. Science and Discovery* **015003**(2), 26pp (2009)
17. Gourdain, N., Gicquel, L., Montagnac, M., Vermorel, O., Gazaix, M., Staffelbach, G., García, M., Boussuge, J.F., Poinot, T.: High performance parallel computing of flows in complex geometries - part 2: applications. *Comput. Science and Discovery* **015004**(2), 28pp (2009)
18. Hasse, C., Sohm, V., Durst, B.: Detached eddy simulation of cyclic large scale fluctuations in a simplified engine setup. *Int. J. Heat Fluid Flow* **30**, 32–43 (2009)
19. Hasse, C., Sohm, V., Durst, B.: Numerical investigation of cyclic variations in gasoline engines using a hybrid URANS/LES modeling approach. *Computers & Fluids* **39**(1), 25–48 (2010)
20. Haworth, D.: Large-eddy simulation of in-cylinder flows. *Oil & Gas Sci. Tech.* **54**(2), 175–185 (1999)
21. Heywood, J.B.: *Internal combustion engine fundamentals*. McGraw and Hill Series in Mechanical Engineering. McGraw-Hill, New-York (1988)
22. Klein, M.: An attempt to assess the quality of large eddy simulations in the context of implicit filtering. *Flow, Turb. and Combustion* **75**(1-4), 131–147 (2005)
23. Klein, M., Meyers, J., Geurts, B.: Assessment of les quality measures using the error landscape approach. In: S. Netherlands (ed.) *Proc. of the Quality and Reliability in Large-Eddy Simulations*, vol. 12, pp. 131–142. Springer-Verlag Berlin (2008)
24. Lacour, C., Pera, C., Énaux, B., Vermorel, O., Angelberger, C., Poinot, T.: Exploring cyclic variability in a spark-ignition engine using experimental techniques, system simulation and large-eddy simulation. In: *Proc. of the 4th European Combustion Meeting*. Vienna, Austria (2009)
25. Lax, P.D., Wendroff, B.: Difference schemes for hyperbolic equations with high order of accuracy. *Commun. Pure Appl. Math.* **17**, 381–398 (1964)
26. Lumley, J.L.: *Stochastic Tools in Turbulence*. Academic Press New York (1970)



27. Maurel, S., Borée, J., Lumley, J.L.: Extended proper orthogonal decomposition: Application to jet/vortex interaction. *Flow, Turb. and Combustion* **67**, 125–136 (2001)
28. Mendez, S., Eldredge, J.: Acoustic modeling of perforated plates with bias flow for large-eddy simulations. *J. Comput. Phys.* **228**(13), 4757–4772 (2009)
29. Moin, P., Apte, S.V.: Large-eddy simulation of realistic gas turbine combustors. *Am. Inst. Aeronaut. Astronaut. J.* **44**(4), 698–708 (2006)
30. Moureau, V., Barton, I., Angelberger, C., Poinso, T.: Towards large eddy simulation in internal-combustion engines: simulation of a compressed tumble flow. SAE Paper (2004-01-1995) (2004)
31. Moureau, V., Lartigue, G., Sommerer, Y., Angelberger, C., Colin, O., Poinso, T.: Numerical methods for unsteady compressible multi-component reacting flows on fixed and moving grids. *J. Comput. Phys.* **202**(2), 710–736 (2005)
32. Nicoud, F., Benoit, L., Sensiau, C.: Acoustic modes in combustors with complex impedances and multidimensional active flames. *AIAA Journal* **45**, 426–441 (2007)
33. Ozdor, N., Dulger, M., Sher, E.: Cyclic variability in spark ignition engines. A literature survey. SAE Paper (950683) (1994)
34. Patel, N., Menon, S.: Simulation of spray–turbulence–flame interactions in a lean direct injection combustor. *Combust. Flame* **153**(1-2), 228–257 (2008)
35. Poinso, T., Lele, S.: Boundary conditions for direct simulations of compressible viscous flows. *J. Comput. Phys.* **101**(1), 104–129 (1992)
36. Poinso, T., Veynante, D.: *Theoretical and Numerical Combustion*. R.T. Edwards, 2nd edition (2005)
37. Richard, S., Colin, O., Vermorel, O., Benkenida, A., Angelberger, C., Veynante, D.: Towards large eddy simulation of combustion in spark ignition engines. *Proc. Combust. Inst.* **31**(3059-3066) (2007)
38. Rudy, D.H., Strikwerda, J.C.: A non-reflecting outflow boundary condition for subsonic Navier Stokes calculations. *J. Comput. Phys.* **36**, 55–70 (1980)
39. Schmitt, P., Poinso, T., Schuermans, B., Geigle, K.P.: Large-eddy simulation and experimental study of heat transfer, nitric oxide emissions and combustion instability in a swirled turbulent high-pressure burner. *J. Fluid Mech.* **570**, 17–46 (2007)
40. Selle, L., Nicoud, F., Poinso, T.: The actual impedance of non-reflecting boundary conditions: implications for the computation of resonators. *AIAA Journal* **42**(5), 958–964 (2004)
41. Sirovich, L.: Turbulence and the dynamics of coherent structures. *Quart. Appl. Math.* **XLV**(3), 561–590 (1987)
42. Smagorinsky, J.: General circulation experiments with the primitive equations: 1. the basic experiment. *Mon. Weather Rev.* **91**, 99–164 (1963)
43. Thobois, L., Lauvergne, R., Poinso, T.: Using LES to investigate reacting flow physics in engine design process. SAE Paper (2007-01-0166) (2007)
44. Toledo, M.S., Penven, L.L., Buffat, M., Cadiou, A., Padilla, J.: Large eddy simulation of the generation and breakdown of a tumbling flow. *Int. J. Heat Fluid Flow* **28**, 113–126 (2007)
45. Tran, N., Ducruix, S., Schuller, T.: Analysis and control of combustion instabilities by adaptive reflection coefficients. In: *Proceedings of the 13th AIAA/CEAS Aeroacoustics Conference*, AIAA Paper, vol. 3716, pp. 21–23 (2007)
46. Vermorel, O., Richard, S., Colin, O., Angelberger, C., Benkenida, A., Veynante, D.: Towards the understanding of cyclic variability in a spark ignited engine using multi-cycle LES. *Combust. Flame* **156**, 1525–1541 (2009)
47. Young, M.B.: Cyclic dispersion in the homogeneous charge spark-ignition engine. a literature survey. SAE Paper (810020) (1981)